Journal of Biomedical Informatics 57 (2015) 74–87

Contents lists available at ScienceDirect

Journal of Biomedical Informatics

journal homepage: www.elsevier.com/locate/yjbin

Simulation of metastatic progression using a computer model including chemotherapy and radiation therapy

Anja Bethge [a], Udo Schumacher [b], Gero Wedemann [a,*]

[a] Competence Center Bioinformatics, Institute for Applied Computer Science, University of Applied Sciences Stralsund, Zur Schwedenschanze 15, 18435 Stralsund, Germany
[b] Experimental Morphology, Center for Experimental Medicine, University Medical Center Hamburg, Martinistrasse 52, 20246 Hamburg, Germany

ARTICLE INFO

Article history:
Received 30 December 2014
Revised 1 July 2015
Accepted 12 July 2015
Available online 17 July 2015

Keywords:
Computer simulation
Metastasis
Radiotherapy
Radioimmunotherapy
Radioembolization
Chemotherapy

ABSTRACT

Introduction: Despite considerable research efforts, the process of metastasis formation is still a subject of intense discussion, and even established models differ considerably in basic details and in the conclusions drawn from them. Mathematical and computational models add a new perspective to the research as they can quantitatively investigate the processes of metastasis and the effects of treatment. However, existing models look at only one treatment option at a time.

Methods: We enhanced a previously developed computer model (called CaTSiT) that enables quantitative comparison of different metastasis formation models with clinical and experimental data, to include the effects of chemotherapy, external beam radiation, radioimmunotherapy and radioembolization. CaTSiT is based on a discrete event simulation procedure. The growth of the primary tumor and its metastases is modeled by a piecewise-defined growth function that describes the growth behavior of the primary tumor and metastases during various time intervals. The piecewise-defined growth function is composed of analytical functions describing the growth behavior of the tumor based on characteristics of the tumor, such as dormancy, or the effects of various therapies. The spreading of malignant cells into the blood is modeled by intravasation events, which are generated according to a rate function. Further events in the model describe the behavior of the released malignant cells until the formation of a new metastasis. The model is published under the GNU General Public License version 3.

Results: To demonstrate the application of the computer model, a case of a patient with a hepatocellular carcinoma and multiple metastases in the liver was simulated. Besides the untreated case, different treatments were simulated at two time points: one directly after diagnosis of the primary tumor and the other several months later. Except for early applied radioimmunotherapy, no treatment strategy was able to eliminate all metastases. These results emphasize the importance of early diagnosis and of proceeding with treatment even if no clinically detectable metastases are present at the time of diagnosis of the primary tumor.

Conclusion: CaTSiT could be a valuable tool for quantitative investigation of the process of tumor growth and metastasis formation, including the effects of various treatment options.

1. Introduction

The formation of cancer metastases has been defined as one of the hallmarks of cancer [1,2]. The clinical importance of metastasis is highlighted by the fact that more than 90% of cancer patients die because of distant metastases and not because of the primary tumor, which can often be treated locally [3]. Despite its clinical importance, metastasis formation remains an enigmatic aspect of cancer biology that is not well enough understood to develop strategies to prevent their formation [4].

As a complement to experimental research and clinical studies, mathematical models are valuable tools for investigating the progress of tumor growth and metastasis and for devising optimal treatment strategies, such as for chemo- and/or radiation therapy. Thus, in recent years a variety of mathematical models have been developed. In 2000 Iwata et al. [5] published a model for the growth and size distribution of multiple metastatic tumors, which

Abbreviations: CaTSiT, cancer and treatment simulation tool; EBRT, external beam radiation therapy; MIRD, Medical Internal Radiation Dose; XML, Extensible Markup Language; XSD, XML Schema Definition.

* Corresponding author. Tel.: +49 3831 457051.
E-mail addresses: anja.bethge@fh-stralsund.de (A. Bethge), uschumac@uke.de (U. Schumacher), gero.wedemann@fh-stralsund.de (G. Wedemann).

http://dx.doi.org/10.1016/j.jbi.2015.07.011
1532-0464/

has since been further investigated, validated and developed by a number of researchers, including Struckmeier [6], Barbolosi et al. [7], Devys [8], Haustein and Schumacher [9], Hartung et al. [10] and Benzekry, who enhanced this model by including the effects of angiogenesis [11] and dormancy [12]. Another mathematical approach was developed by Newton et al. [13,14], who calculated a transition matrix using a stochastic Markov chain model to describe the growth of primary lung cancer and the spread of metastases to distant sites.

Further models have been developed that also modeled chemo- and radiation therapy. The effects of cytotoxic drugs on tumor growth were modeled by Wheldon [15], Birkhead [16,17], Usher [18], Panetta [19–21] and Dua [22], for example. Chemotherapy in combination with antiangiogenic drugs was modeled by d'Onofrio [23] and Benzekry [24], while de Pillis examined the combination of chemotherapy with immunotherapy [25]. Models describing the effects of radiation therapy were developed by Wang [26], Bernhardt [27,28], Wheldon [29] and Leder [30], among others. However, in radiation therapy the use of mathematical models has been limited mainly to calculating optimal doses [27,28] or obtaining optimal treatment schedules [30,31].

For the analysis of data from mouse models or clinical studies, it is important to include the effects of different treatment modalities on the same case, because several treatment modalities are often combined in practice. In this article a computer model, named CaTSiT (cancer and treatment simulation tool), is presented that enables commonly applied treatment options to be simulated. The original model was published in [32], where it was used to compare two models of metastatic progression, the linear and parallel progression model [33], in a case of a hepatocellular carcinoma. The comparison of the simulated data with the clinical data revealed that in this particular case metastasis formation is an early event and only the first metastases seeded from the primary tumor contribute significantly to the tumor burden and thus cause the patient's death, if he is left untreated. In [34] the computer model was used to analyze the experimental data of an HT29 human colon cancer xenograft mouse model. In this context the computer model was enhanced to model dormancy. The simulation results showed that natural killer cells decelerate the growth of the primary tumor, kill 80% of the circulating tumor cells that could have otherwise established a new metastasis and hamper the establishment and proliferation of the malignant cells in distant tissue, possibly because of an induction of dormancy in disseminated tumor cells.

In the work presented here the computer model was further enhanced to model different treatment modalities. Besides the already implemented complete resection of the primary tumor, the computer model was now enhanced to model partial resection and two other commonly applied treatments: chemotherapy and external beam radiation. Furthermore, two specialized treatments were added to the computer model: radioimmunotherapy and radioembolization. In this process the original computer model was slightly modified by introducing a piecewise-defined growth function to facilitate the model and its implementation.

As a demonstration the application of the enhanced computer model is represented in the results section on the data of one patient with hepatocellular carcinoma und multiple metastases in the liver.

Owing to the structure of the computer model and the software, it is easy to extend CaTSiT to include further new findings about metastatic progression and novel treatments in the future. CaTSiT is available as open source software under the GNU General Public License version 3. To our knowledge no existing software package can provide a similar wide range of functionality.

2. Methods

2.1. Compartments and events

The basic structure of the computer model was first described in [32] and [35]: It is developed as a building kit [32] that provides different kinds of building blocks, from which various simulation setups can be assembled [30,33]. The two main types of building blocks are compartments and events. A compartment describes a physical entity that can contain malignant cells; it can be, for example, the primary tumor, the bloodstream or a metastasis [32]. An event describes what occurs in a compartment at a specific time. In contrast to [32] and [35], events now can have either local or global effects: local events influence only one compartment, whereas global events can affect more than one compartment. Global events are mostly used to describe therapies such as radiation therapy. Local events are further subdivided into events that influence the whole compartment, such as dormancy or resection of the primary tumor, and events that affect tumor progression, such as cell division, apoptosis and cell transfer (e.g. intravasation and extravasation).

Compartments can be modeled either discrete or continuous [32]. In a continuous compartment, all internal processes are modeled by continuous mathematical functions. The growth of the compartment size is described by a growth function and the spread of malignant cells by a colonization rate, which depends on the size of the compartment and therefore on its growth function. The growth function and colonization rate can be parameterized individually for different compartments, for instance the primary tumor and different kind of metastases. Larger compartments, such as the primary tumor and metastases, are usually modeled as continuous compartments [32].

In a discrete compartment, all internal processes are modeled with discrete tumor progression events. The increase or decrease in the number of malignant cells in a discrete compartment is modeled by simulating each cell division, apoptosis or translocation into a different compartment. One can think of a discrete compartment as a bucket, which cells can be placed into or removed from. For each discrete compartment a set of possible event types can be defined, and associated with each event is a probability of occurrence (see Fig. 1). Discrete compartments are mostly used to model the bloodstream [32,35].

With these building blocks, various simulation setups can be constructed to investigate different scenarios of metastatic progression and treatment strategies. A sample setup involving an untreated hepatocellular carcinoma with metastases in the liver and the lung is shown in Fig. 1.

2.2. Modeling tumor growth using a continuous compartment

In a continuous compartment that models the primary tumor or a metastasis, the growth function $x(t)$ represents the number of cells in the tumor at time t and is the solution of

$$\frac{dx}{dt} = g(x), \quad x(0) = N_0, \tag{1}$$

where the parameter N_0 is the number of cells at time $t = 0$. When modeling tumor growth in a human patient, N_0 is taken to be 1, because it is assumed that the primary tumor or a metastasis starts as a single malignant cell [5,36–38]. When modeling experimental data, such as data from a mouse model, N_0 could be the number of cells injected into the mouse, for instance.

Different functions can be chosen for the growth rate $g(x)$, such as linear, exponential or power laws. Most tumors exhibit a Gompertzian growth rate, which is given by

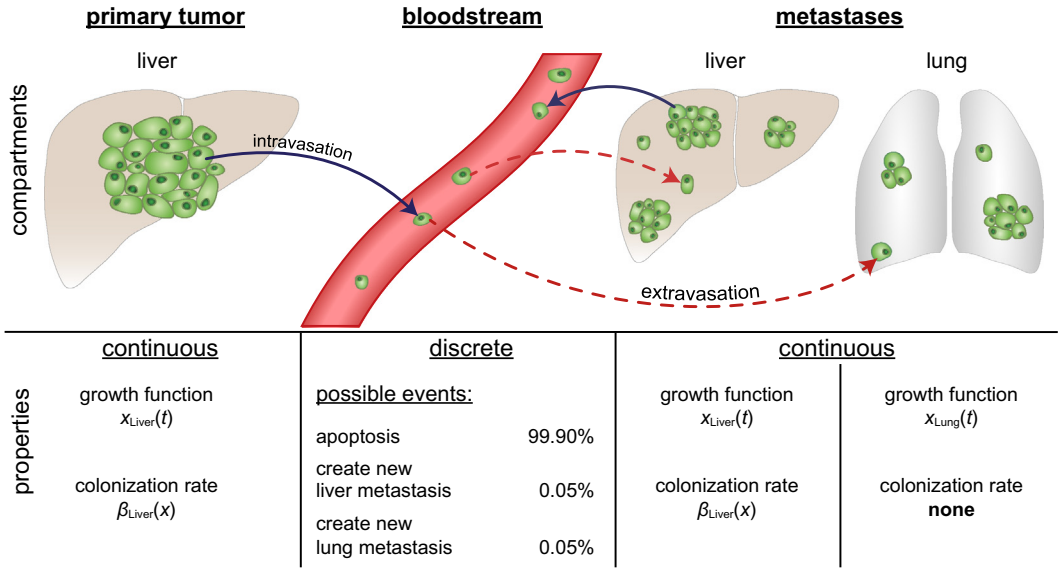

Fig. 1. Sample simulation setup for a hepatocellular carcinoma with metastases in the liver and the lung. In this sample simulation setup, the primary tumor is located in the liver and spreads metastases within the liver and into the lungs. The primary tumor and the metastases are modeled as continuous compartments and the bloodstream is modeled as a discrete compartment. The primary tumor and the liver metastases grow with the same growth function $x_{Liver}(t)$. Intravasation events (blue solid arrows), whereby a single malignant cell enters the bloodstream, are generated according to the colonization rate $\beta_{Liver}(x)$. Lung metastases grow according to the growth function $x_{Lung}(t)$ and do not spread malignant cells into the blood. The possible events that can occur in the bloodstream are listed below the bloodstream along with their associated probabilities. Most cells in the bloodstream die, and only few can create a new metastasis in either the liver or the lung (red dashed arrows). The probabilities of the events were chosen arbitrarily for demonstration and do not claim to reflect biological reality in the patient. (For interpretation of the references to color in this figure legend, the reader is referred to the web version of this article.)

$$g(x) = ax \ln\left(\frac{b}{x}\right) \tag{2}$$

where a is the growth rate constant and b represents the maximum size of the tumor [5]. Taking Eq. (2) as the growth rate $g(x)$ in Eq. (1), integrating the resulting equation over x and applying the boundary condition stated in Eq. (1), the number of cells in the tumor at time t is given by

$$x(t) = b\left(\frac{b}{N_0}\right)^{-e^{-at}} \tag{3}$$

See Fig. S1-A In The Supplementary Material for the graph of this function. Other growth functions, arising from linear and exponential growth rates can be found in Table S1 in the Supplementary Material.

2.3. Modeling tumor spread from continuous compartments

In a continuous compartment the primary tumor and its metastases spread single malignant cells at a colonization rate [5] which is given by the following function of the tumor size:

$$\beta(x) = mx^{\delta} \tag{4}$$

The parameter m is the colonization coefficient, and δ is the fractal dimension of blood vessel infiltration into the tumor; hence, δ describes how well the tumor is supplied with blood. A value of 1 for δ signifies that the tumor is completely supplied with blood while a value of 2/3 indicates that the tumor is only superficially supplied with blood. To compute the time of the next intravasation event, the colonization rate is numerically integrated over time, using Eq. (3) for the number of cells in the tumor, until the integral reaches the value ζ. Since it seems not realistic, that the time between two intravasation events is a fixed value, ζ is computed for each single intravasation event randomly in the interval between 0 and 2 using the *Mersenne Twister* [39] random number generator [35].

2.4. Modeling dormancy and late dormancy

Metastases can stay dormant for a certain length of time before they start to grow according to their growth function. To model initial dormancy of a new metastasis, upon its creation (from a single cell) its state is set to dormant. In contrast to [34] the growth function is replaced by a constant function returning the value 1 (see Fig. S1-B in the Supplementary Material). In this phase no tumor progression events can be executed or created for this compartment. At the end of the dormancy phase, the state of the compartment is reset and the compartment starts to grow according to the growth function in Eq. (1). Since it is unlikely that all metastases remain dormant for the identical time span the length of the dormancy phase is computed randomly for each metastasis using a random number generator. The distribution of these random values can be parameterized as either normal distribution with mean and standard deviation or uniform distribution with an interval [34]. This parametrization makes it possible to evaluate the effects of different models of dormancy.

To model late dormancy, the tumor first grows according to the growth function in Eq. (1) until it reaches a certain size ds. The tumor is then switched to a dormant state, where similar to initial dormancy the growth function is replaced by a constant function returning the tumor's size at the start of the late dormancy phase (see Fig. S1-C in the Supplementary Material). After the end of the late dormancy phase, the tumor resumes growing according to the growth function. In contrast to [34], the accrued offset is not incorporated by an additional time parameter but by assigning a new start size $N_0 = ds$ to the growth function (see Fig. 2B). Since it is unlikely that all metastases switch into late dormancy having the identical number of cells, the start size of the late dormancy

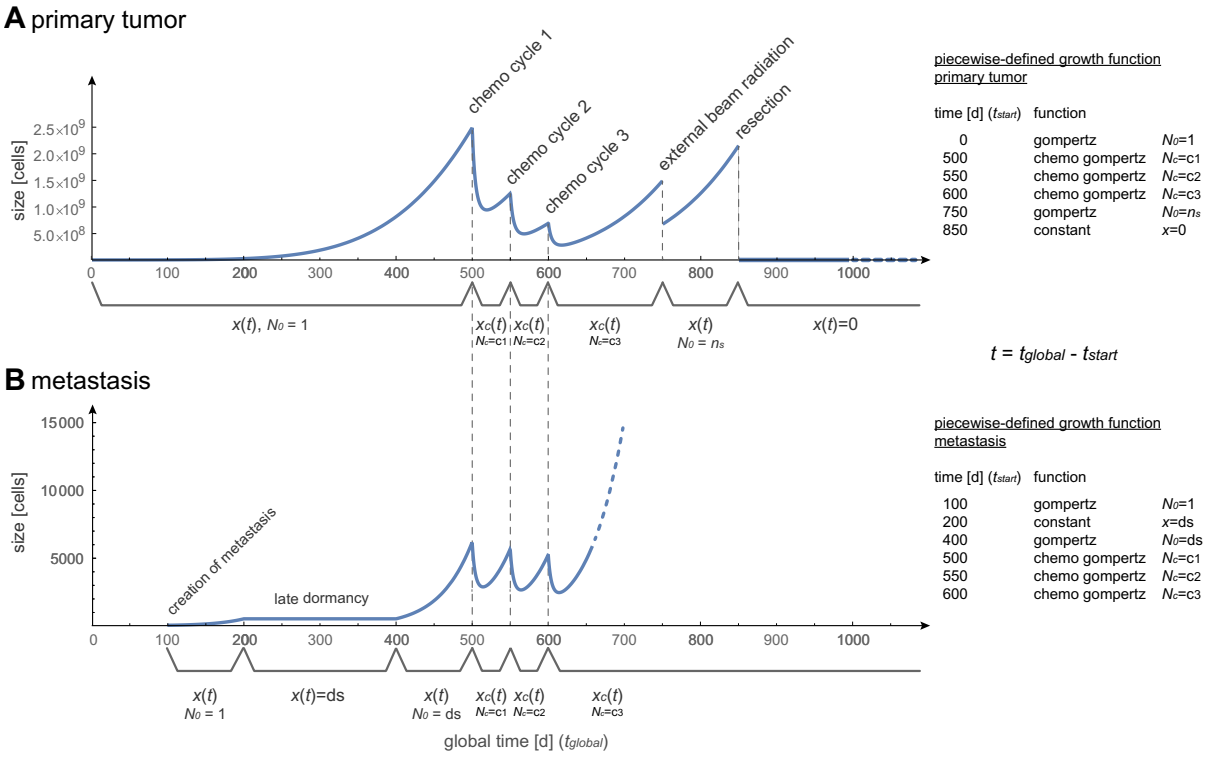

Fig. 2. Example of a piecewise-defined growth function for the primary tumor and one metastasis. Graphs of growth over time (left) and details of the piecewise-defined growth functions (right) for a primary tumor (A) and one metastasis (B). (A) The primary tumor is created at the global simulation time 0 and starts growing from a single cell ($N_0 = 1$) according to a Gompertzian function. On days 500, 550 and 600 chemotherapy is applied to the whole simulated system, during which the current growth function is replaced by a modified chemotherapy growth function ($x_c(t)$). On day 750 external beam radiotherapy is applied to the primary tumor, followed by the resection on day 850. (B) The metastasis is created at global simulation time 100. Similar to the primary tumor, it is created from a single cell ($N_0 = 1$) and grows with a Gompertzian growth rate. After reaching a size $ds = 503$ cells, it switches to a dormant state for 200 days. Afterward, the metastasis continues growing according to the initial Gompertzian growth function but with an updated value of $N_0 = ds$. At the global time points 500, 550 and 600 the metastasis is affected by the chemotherapy. Afterward, the metastasis continues growing unimpeded. The valid time t for each component function of the piecewise-defined growth function is obtained by subtracting the start time t_{start} of the currently valid function from the global time t_{global}.

is computed randomly following a parameterizable distribution that can either be normal or uniform [34]. The time-span of the late dormancy phase is parameterized similarly to that of initial dormancy.

2.5. Modeling therapies

Besides the progression of the primary tumor and its metastases, three of the most commonly applied treatments (resection of the primary tumor, chemotherapy and external beam radiotherapy) as well as two more specialized treatments (radioimmunotherapy and radioembolization) were implemented.

2.5.1. Resection of the primary tumor

In an ideal treatment the primary tumor is removed completely during the resection. In these cases, in a discrete compartment, resection is modeled by setting the number of cells in the primary tumor compartment to zero. All cell progression events assigned to the primary tumor that have not yet been executed at the time of the resection are deleted from the event list. In a continuous compartment, the growth function is replaced by a constant function returning the value 0 for the number of cells (see Fig. S1-D in the Supplementary Material). Consequently, the colonization rate will also become zero, and no more intravasation events will be created that originate from the primary tumor.

However, complete resection of the primary tumor may not always be possible. In this case the number of the remaining cells is computed via a parameterizable remnant fraction. If the primary tumor is modeled as a discrete compartment then the number of cells is reset to the number of remaining cells. In contrast to complete resection, only a part of the cell progression events that have not been executed up to the time of the resection are deleted from the event list according to the remnant fraction. E.g., if 10 cell division events of the primary tumor were present in the event list before the resection and 90% of the cells in the primary tumor were removed during the resection, then 9 of those cell division events will be deleted from the event list to account for the decreased number of cells.

In a continuous compartment, the growth function is replaced by a modified version of the original growth function, with the initial size N_0 set to the number of remaining cells.

2.5.2. Chemotherapy

Simulation of chemotherapy is currently available only for continuous compartments in our computer model. It is modeled by a modified growth function $x_c(t)$, which is the solution of

$$\frac{dx}{dt} = g(x) - f\mu c(t)x, \quad x_c(t_c) = N_c \tag{5}$$

Here $g(x)$ is the growth rate of the tumor, just as in Eq. (1) [15]. The parameter f is used for cycle-specific chemotherapy [40] and describes the fraction of cells that are in a cell-cycle phase affected by the chemotherapy; if the chemotherapy is not cycle-specific and thus affects all cells similarly regardless of their cell-cycle state, f is assigned a value of 1. The parameter μ describes the drug sensitivity of the cells and therefore the effectiveness of the chemotherapy, and $c(t)$ models the drug concentration in the tumor. In this work

an exponential decay of the drug concentration, with a decay rate $\gamma = \ln(2)/T_{1/2}$ [25], where $T_{1/2}$ denotes the half-life of the drug, was assumed, so that

$$c(t) = e^{-\gamma t} \tag{6}$$

The parameter N_c in Eq. (5) is the number of cells at time t_c, the start time of the chemotherapy cycle.

Upon substituting Eq. (2) for the growth rate $g(x)$ and Eq. (6) for the drug concentration in Eq. (5) and then solving, the following modified growth function $x_c(t)$ is obtained:

$$x_c(t) = e^{\left(\frac{f\mu\left(e^{-\alpha t}-e^{-\gamma t}\right)}{\alpha-\gamma}\right)} b\left(\frac{b}{N_0}\right)^{-e^{-\alpha t}} \tag{7}$$

See Fig. S1-E in the Supplementary Material for the graph of this function.

If the compartment is in a dormant state when chemotherapy is applied, the treatment has no immediate effect. Instead, after the end of the dormancy phase a delayed version of the growth function under chemotherapy is applied, in which the drug concentration is decreased by an amount dependent on the time span between the chemotherapy and the end of the dormancy phase. This growth function for delayed chemotherapy, as well as further chemotherapy growth functions for linear and exponential growth rates, can be found in Table S1 in the Supplementary Material.

2.5.3. External beam radiation therapy

Each application of external beam radiation therapy (EBRT, or teletherapy) to the primary tumor is modeled as a single incident in time, after which the number of surviving cells, n_s, is computed according to the linear quadratic model

$$n_s = n_b e^{-\alpha D-\beta D^2} \tag{8}$$

where n_b is the number of cells in the tumor before treatment and D is the radiation dose administered to the tumor during the treatment session. The parameters α and β are tissue constants that describe the radiosensitivity of the cells being radiated. For example, rapidly proliferating tissues, such as mucosa, are much more radiosensitive and will respond to considerably lower doses than slowly proliferating tissues, such as bone tissue, which may sustain higher doses of radiation before they are affected. Simply put, α can be regarded as the probability, per absorbed dose, of creating a lethal double-strand break in the DNA that leads to cell death [41], whereas β can be considered as the probability of inducing two single-strand breaks in short succession, resulting in a lethal double-strand break [41].

After application of EBRT to a discrete compartment, the number of tumor cells is set to the number of surviving tumor cells n_s. Similar to the partial resection of the primary tumor, cell progression events assigned to the primary tumor that have not been executed up to the time of the therapy are partially deleted from the event list according to the survival rate n_s/n_0.

In a continuous compartment, after EBRT the growth function is replaced by a modified version of the original growth function, with the initial size N_0 set to the number of surviving cells n_s (see Fig. 2A and Fig. S1-F in the Supplementary Material). If the compartment is in a dormant state while radiation therapy is applied, the constant function during dormancy and the initial condition of the subsequent growth function are updated to the number of surviving cells n_s.

2.5.4. Radionuclide therapy

In addition to standard EBRT, two more specialized therapies from the field of nuclear medicine were implemented in the computer model.

2.5.4.1. Radioimmunotherapy.

In radioimmunotherapy the radionuclide is combined with an antibody that binds to a tumor-associated antigen to deliver a lethal dose of radiation directly to the tumor cells [42,43]. In this way, a higher dose can be delivered to the tumor while the effects on normal tissue are minimized. In contrast to EBRT, small and as-yet-undetected metastases can be treated with radioimmunotherapy as well. However, this is an idealized situation. Recent studies [44,45] have revealed that in solid tumors, only a very small proportion of the antibodies can infiltrate the tumor and thus deliver the radiation activity to the tumor cells.

The number of surviving tumor cells, n_s, is computed similarly to EBRT, using Eq. (8). Because the radionuclide is brought directly into the body and then spreads to the targets, the dose D that is finally administered to the single tumors depends on properties of the applied radionuclide as well as on the administered activity. It is computed using the following formula derived from the Medical Internal Radiation Dose (MIRD) Schema [46,47]:

$$D = \frac{A_t T_e E}{m_t \ln(2)} \tag{9}$$

The detailed derivation can be found in the supplementary material. The parameter m_t represents the mass of the tumor, E the average energy of the radionuclide per disintegration and A_t the effective activity in the tumor. It is assumed that the radiation is absorbed instantly and fades from the system exponentially at a rate depending on the effective half-life T_e, which is a combination of biological half-life (T_b) and physical half-life (T_p):

$$T_e = \frac{T_b\, T_p}{T_b + T_p} \tag{10}$$

Radioimmunotherapy is modeled as a global event. For each compartment, i.e. the primary tumor and all metastases, the number of surviving cells n_s is computed as described above with Eqs. (8)–(10). For this purpose, the effective activity A_t in each compartment is obtained by distributing the administered activity to the individual tumors in proportion to their size and applying a clearance fraction, which describes the proportion of the administered activity that does not contribute to the therapy because it is not delivered into the individual tumor. After application of therapy, the number of cells is reset or the growth function updated, respectively, for discrete or continuous compartments, similar to EBRT.

2.5.4.2. Radioembolization.

Radioembolization, or selective internal radiation therapy (SIRT), is a therapy specific for hepatocellular carcinoma and local metastases within the liver. It is primarily used when the tumor is non-resectable [48]. The radionuclide (usually Yttrium 90) is injected into the tumor through the hepatic artery and delivered via small glass microspheres that then become trapped in the capillary vessels of the tumor. In this way the tumor can be irradiated from the inside while the toxicity to normal liver tissue is minimized [48,49].

Given that the microspheres are brought directly into the blood vessels of the tumor by the radiologist, only those tumors that are detectable and connected to a blood supply can be treated. Thus, very small and not-yet-detected metastases are not affected by this kind of treatment.

The mean absorbed dose depends on properties of the applied radionuclide and the administered activity and is computed in the same way as in radioimmunotherapy, except that, because the glass microspheres remain in the tissue, the biological half-life is ignored. Furthermore, only compartments that exceed a certain size, $x_{\min}$, are treated. The size $x_{\min}$ can be specified as either a diameter or a volume. If a diameter is specified, the computer model assumes the tumor to be a sphere and computes its

volume accordingly. The number of cells is then computed by assuming that a tumor with a volume of 1 mm^3 contains 10^6 cells [50].

In any of the treatments, if the number of cells $x(t)$ falls below the value 1, the tumor is regarded as extinguished. Hence, as in the resection simulation, the growth rate is replaced by a constant function that returns the value 0, all associated events are removed from the event list and the colonization rate is set to zero.

2.6. Piecewise-defined growth function

As detailed above, different functions are used to describe the growth of a continuous compartment, the effects of various therapies, and certain characteristics of the tumor, such as dormancy. Thus, over its entire lifespan in the simulation, the growth of a continuous compartment can be described by more than one function. The universal growth function of a continuous compartment is a piecewise-defined function composed of different continuous functions that describe the growth behavior of the compartment during different time periods (see Fig. 2). This piecewise-defined growth function is implemented as a list in the computer model, and different functions can be added to the list at various points in time. These time points are always referenced with respect to the global time of the current simulation. Hence, the start time of the first component function of the piecewise-defined growth function is always the creation time of the corresponding compartment, e.g. day 0 for the primary tumor or day 100 for the first metastasis (see Fig. 2). In this way it is easy to obtain the correct time value for evaluating the currently valid function by taking the current global time and subtracting the start time of the current function.

An example of a piecewise-defined growth function for the primary tumor and one metastasis is shown in Fig. 2: The primary tumor is created at the global simulation time 0. It starts as a single cell ($N_0 = 1$) and grows unimpeded according to a Gompertzian function until day 500. On days 500, 550 and 600 chemotherapy is applied to the whole simulated system. At these time points the initial growth function is replaced by a modified chemotherapy growth function that describes the effect of the chemotherapy on the compartment. On day 750 external beam radiotherapy is applied to the primary tumor. The number of surviving cells (n_s) is computed according to Eq. (8), and the chemotherapy growth function is replaced by the initial Gompertzian growth function with an updated value of N_0. Eventually the primary tumor is resected at day 850. At this time point the growth function is replaced by a constant function returning the value 0. At global simulation time 100, the first metastasis is created from a single cell ($N_0 = 1$) and starts growing with a Gompertzian growth rate (Fig. 2B). When the metastasis reaches a size of 503 cells, it switches to a dormant state for 200 days. Hence, between the global time points 200 and 400, the non-existent growth is modeled by a constant function that returns the size of the tumor at the start of the dormancy phase ($ds = 503$). After the dormancy phase, the metastasis continues growing according to the initial growth function but with an updated value of N_0. Because chemotherapy is a systemic therapy, the metastasis is also affected by the chemotherapy cycles at the global time points 500, 550 and 600. Similar to the primary tumor, the initial growth function is replaced by a modified chemotherapy growth function. The subsequent treatments at time points 750 and 850 were applied only to the primary tumor and have no effect on the metastasis. Hence, the metastasis continues growing unimpeded after the third chemotherapy cycle.

As displayed in Fig. 2A the progression of the piecewise-defined growth function does not have to be continuous (resection of the primary tumor) or differentiable at every point. Since only the integral is used to compute the time of new events, these characteristics are insignificant.

For every continuous compartment in the simulation, its piecewise-defined growth function is generated individually upon creation of the compartment. Therefore, the progression of the piecewise-defined growth function for each compartment is computed independently in advance, taking into account all parameterized characteristics and treatments. An exception is the simulation of radioimmunotherapy. For this treatment, the mean absorbed dose and thus the number of surviving cells cannot be computed in advance independently of other compartments because, as explained above, the effective activity is distributed to the individual tumors according to their relative size, so that the total mass of the primary tumor and all metastases is needed. Although it is possible to compute in advance the number of cells in all existing tumors, the same cannot be done for tumors that are yet to be created in the time period between the creation of the current tumor compartment and the application of radioimmunotherapy. Thus, in this case the piecewise-defined growth function is updated at the time of radioimmunotherapy by the corresponding event, and then the progression of the piecewise-defined growth function is recalculated starting from this time point.

2.7. Simulation procedure

Simulation setups are configured in the XML (Extensible Markup Language) format. An XML Schema Definition (XSD) describes the structure of the configuration file. In this file, the building blocks (e.g. the primary tumor, bloodstream and metastases) and their properties (e.g. growth function, colonization rate and cell progression events) are parameterized. Treatments to be applied are also defined and parameterized in this file.

CaTSiT parses the configuration file and creates all the necessary compartments with their associated properties, as well as all events that can already be determined from the configuration, such as treatments or the start and stop of a (late) dormancy phase.

All events are stored in an event list and are executed in sequence according to the global time points at which they occur. The simulation starts with the creation and execution of the first tumor progression event. When an event is executed, the compartment is changed according to the event type. For example, during a cell division event the number of cells in the compartment is increased by one, whereas after a resection event the number of cells is set to zero or the number of cells remaining in the tissue, respectively. If the actual event is a tumor progression event, then a new event is created according to the defined set of event types for the compartment and the associated probabilities. The time of the newly created event is computed from a mean time function and a distribution which is used to model variance in the computation of the time value. Both, the mean time function and the distribution can be parameterized separately for each tumor progression event in the event set. In this way new events are continually created and executed. The simulation stops when a pre-specified time span has been covered.

During the simulation, the current state of the system is regularly saved in a spreadsheet. The following values are saved: time in minutes and in days, number of cells in the primary tumor, number of cells in the bloodstream, number of metastases, number of cells in all metastases, and a size histogram of all the metastases. If metastases occur in more than one host organ, the simulation can be configured to save information about the number of metastases, cells and the size histogram of metastases individually for each host organ.

Usually, each simulation setup is computed about 100 times. After completion of all simulation runs for a given setup, the mean

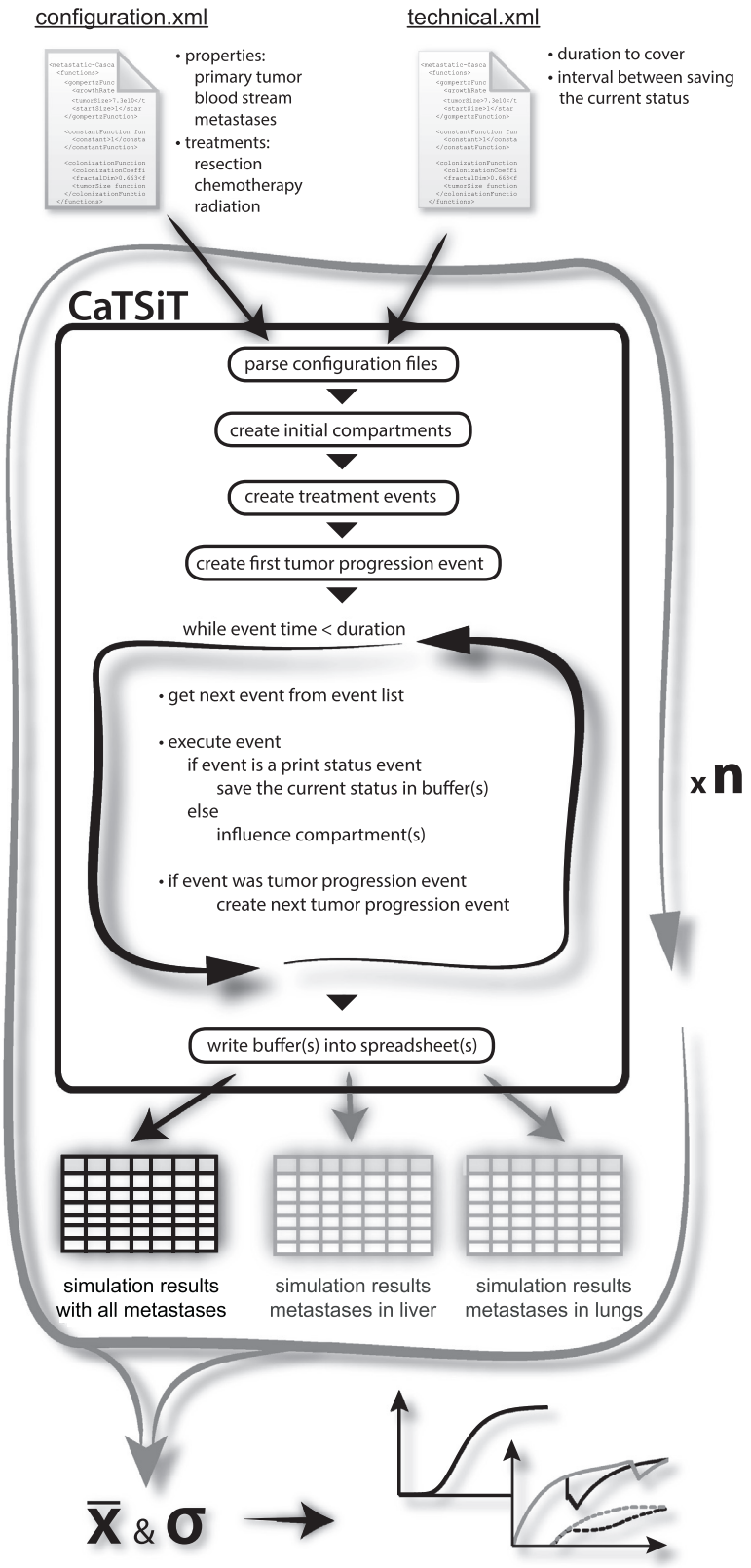

Fig. 3. Simulation procedure. Simulation setups, including the properties of all compartments and treatments, are configured in a XML (Extensible Markup Language) file (configuration.xml). Technical information such as the duration the simulation shall cover and the interval in which the current state of the simulated system shall be saved are parametrized in a separate XML file (technical.xml). The CaTSiT software (black frame) parses both files, creates all necessary compartments and events and starts the simulation by creating the first tumor progression event. Events are stored by time in an event list. One by one, the next event is retrieved from the event list and executed until the parametrized time span was covered. According to its parametrization an event influences one or more compartments. If it is a tumor progression event, than a new event is created after the execution to describe what happens next in the corresponding compartment. The current status of the system, including current time, size of the primary tumor, number of metastases and a size histogram of all metastases is saved periodically in a buffer which is written in a spreadsheet file at the end of the simulation. If parametrized in the configuration file, separate result files can be created for each organ. To create variance, a single simulation setup is simulated several times. Afterward, mean and standard deviation are computed, which than can be used to analyze and visualize the simulation results.

Table 1
Parameter values used in the sample simulation setups.

Parameter	Name	Value	Source
Tumor growth			
a	Growth rate constant	0.00286 day^{-1}	Iwata [5]
b	Maximum size of tumor	7.3×10^{10} cells	
m	Colonization coefficient	5.3×10^{-8} $(cell\ day)^{-1}$	
δ	Fractal dimension of blood vessels	0.663	
Chemotherapy (7 cycles in an interval of 14 days [25])			
f	Fraction of tumor cells in S-phase	0.26	Pourgholami [51]
μ	Fraction of tumor cells killed by chemotherapy	0.9	Morris [52]
γ	Drug decay rate	0.92 day^{-1}	Derived from de Pillis [25] and Chan [53]
External beam radiation therapy			
α	Radiosensitivity	0.35 Gy^{-1}	Bernhardt [28]
β	Radiosensitivity	0.023 Gy^{-1}	derived from Tai [54]
D	Administered dose	36 Gy in daily 2 Gy fractions, 5 times a week	Zeng [55], Huang [56], Cupino [57]
Radioimmunotherapy with ^{131}I (Iodine 131) labeled antibodies			
A_0	Administered activity	0.93 GBq	Zeng [55]
	Clearance fraction	0.9	Heine [44,45]
E	Average energy per disintegration	0.1818 MeV/(Bq s)	Eckerman [58]
T_p	Physical half-life of radionuclide	192.48 h	Eckerman [58]
T_b	Biological half-life of radionuclide	66 × 24 h	Kramer [59]
Radioembolisation with ^{90}Y (Yttrium 90)			
A_0	Injected activity	0.5 GBq	Kennedy [48]
E	Average energy per disintegration	0.9337 MeV/(Bq s)	
T_p	Physical half-life of radionuclide	64.2 h	
x_{min}	Minimum size for treatment	65.45 mm^3 (diameter 5 mm)	Derived from Iwata [5]

and standard deviation of the results are computed. This simulation procedure is also displayed in Fig. 3.

CaTSiT is publicly available as open source software under GNU General Public License version 3 (GPL-3.0), and can be obtained from http://bioinformatics.fh-stralsund.de/catsit/. On this website, binary and source files of the software are presented together with a detailed description of the software and the XML Schema, sample configuration files, and instructions for installing and using CaTSiT.

3. Results

To demonstrate the broad possibilities of the computer model, various simulation setups for the case of a patient with hepatocellular carcinoma and multiple metastases in the liver were simulated. The data of this patient was published by Iwata et al. [5]. As in the simulation setup shown in Fig. 1, the primary tumor and metastases were modeled as continuous compartments and the bloodstream was modeled as a discrete compartment, but in this case the primary tumor spreads into the liver only. To save on computation time, the colonization rate was parameterized to include only those cells that survive in the bloodstream and eventually create a metastasis. Hence, in this simulation setup the set of possible events that can occur in the bloodstream includes only one event: the creation of a new liver metastasis. Dormancy was not included in the simulations since there was no evidence that dormancy occurred in this patient. As already demonstrated in [35] and [32], this simulation setup can reproduce the clinical data of this one particular patient.

This simulation setup for the untreated case was now used as a basis to simulate different treatments for this patient, such as resection of the primary tumor, EBRT applied to the primary tumor, cycle-specific chemotherapy, cycle-nonspecific chemotherapy, radioimmunotherapy with Iodine 131-labeled antibodies, radioembolization with Yttrium 90, and a combination of primary tumor resection and cycle-nonspecific chemotherapy.

Although chemotherapy is not a standard treatment regime in hepatocellular carcinoma, we still included this treatment option in the simulations, to demonstrate the capabilities of the computer model, since it can easily be parametrized for other types of cancer where chemotherapy is a standard treatment option. Treatments were applied on day 700, which is about a month after the initial diagnosis of the primary tumor, and on day 1500, to study the differences between tumors diagnosed and treated early and those diagnosed and treated late. Treatments were simulated for the case where metastases themselves can metastasize and for the case where only the primary tumor can spread metastases. The parameters for the various simulation setups were taken from the literature and are listed in Table 1.

Altogether, 30 different simulation setups were simulated. The results of the simulations are shown in Figs. 4 and 5, which show the mean values of 100 simulation runs for each single simulation setup. On day 700, the primary tumor had a size of approximately 2.5×10^9 cells, and about 10 metastases with a standard deviation of $\sigma = 2$ metastases were present. In contrast, on day 1500 the primary tumor had a size of 5.2×10^{10} cells, and the number of metastases present was 1117 ($\sigma = 83$), in the case where metastases themselves can metastasize, or 330 ($\sigma = 10$), in the case where only the primary tumor can metastasize.

If treatment commences early, resection of the primary tumor leads to temporary (Fig. 4A) or complete (Fig. 5A) stagnation in the number of metastases. In contrast, if treatment commences late, resection of the primary tumor has almost no effect on the number of metastases if metastases themselves can metastasize (Fig. 4A). If metastases cannot metastasize, the number of metastases stagnates after resection of the primary tumor (Fig. 5A). However, in both cases the total tumor burden is barely affected, because at day 1500 the metastases already constitute the majority of the tumor burden (Figs. 4A and 5A). The results in Figs. 4 and 5 show the ideal case in which all tumor cells of the primary tumor could be removed during resection. Simulations with a remnant fraction of 0.1% were also performed and are shown in Fig. S3 in the Supplemental Materials. Especially, in those simulation setups where metastases are not able to metastasize and the treatment started early at day 700 the remnant has a major impact on the number of metastases. In contrast to complete resection as shown

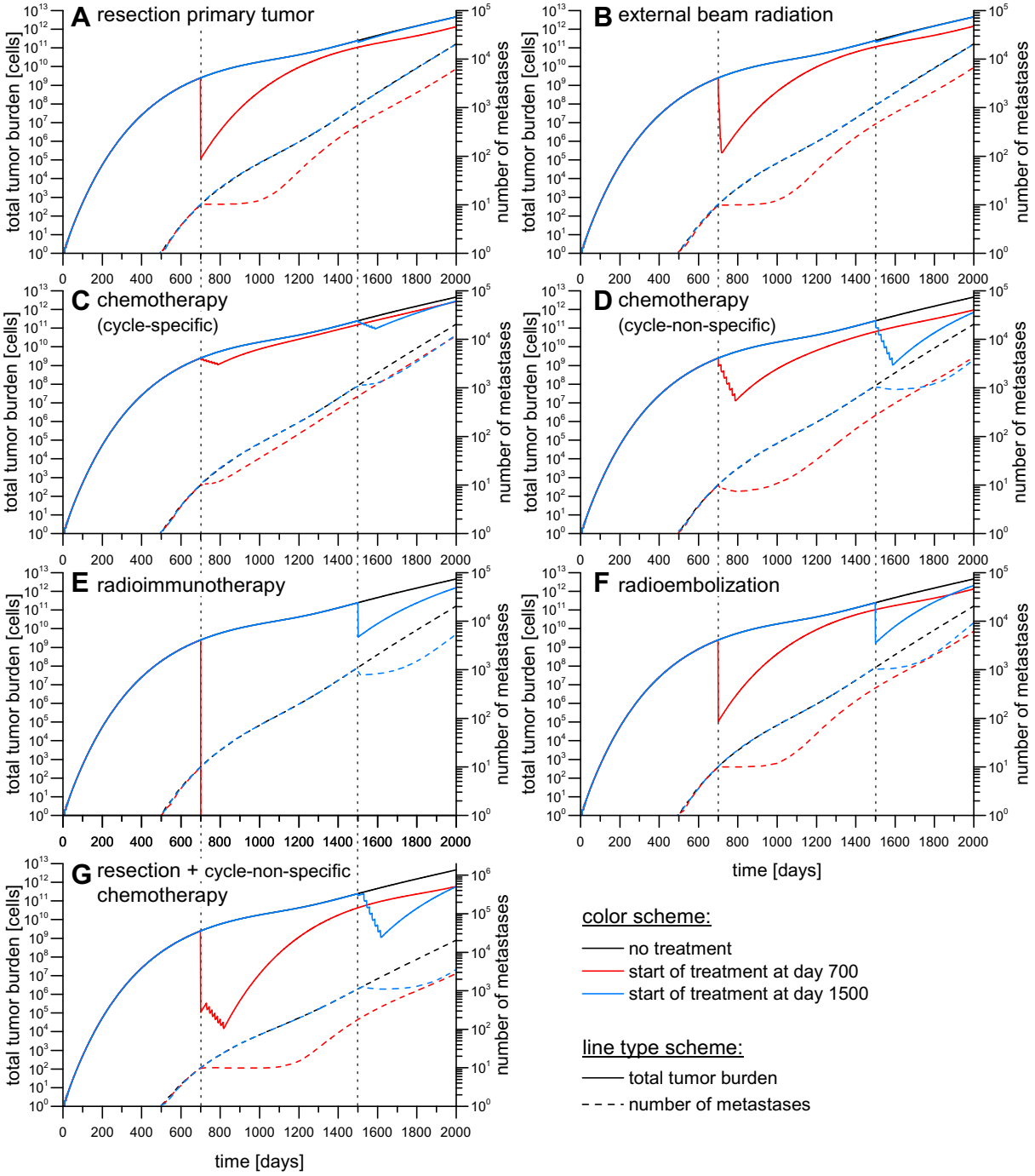

Fig. 4. Simulation results for different treatments for the simulation setups where metastases are able to metastasize. The graphs A–G display the number of metastases (dashed lines, right *y*-axis) and the total tumor burden (solid lines, left *y*-axis) over time, for the untreated course (black lines in panels A–G) and seven simulated treatments: (A) resection of the primary tumor (PT), (B) EBRT of the primary tumor, (C) cycle-specific chemotherapy, (D) cycle-nonspecific chemotherapy, (E) radioimmunotherapy, (F) radioembolization, and (G) a combination of primary tumor resection and cycle-nonspecific chemotherapy. Treatments were started once shortly after diagnosis of the primary tumor on day 700 (red lines) and once on day 1500 (blue lines). In the panels A and B the untreated course is masked by the simulation results of the treatment started at day 1500. (For interpretation of the references to color in this figure legend, the reader is referred to the web version of this article.)

in Fig. 5B the number of metastases starts rising again after some time after the remnant of the primary tumor was able to recover and regrow to a size at which the recurrence was able to spread metastases again (see Fig. S3B).

Although EBRT cannot completely eliminate the primary tumor, it reduces its volume considerably. Hence, if treatment is applied early, the number of metastases stagnates for some time after treatment before starting to rise again (Figs. 4B and 5B). In the late treatment case, similar to resection of the primary tumor, EBRT has almost no impact on the total tumor burden.

Cycle-specific chemotherapy has little direct effect on the number of metastases. Because only 26% of the cells are in the cell-cycle phase that responds to the treatment, only very small metastases established during or shortly before the individual chemotherapy cycles are eliminated. Cycle-nonspecific chemotherapy eradicates slightly more metastases than does cycle-specific chemotherapy.

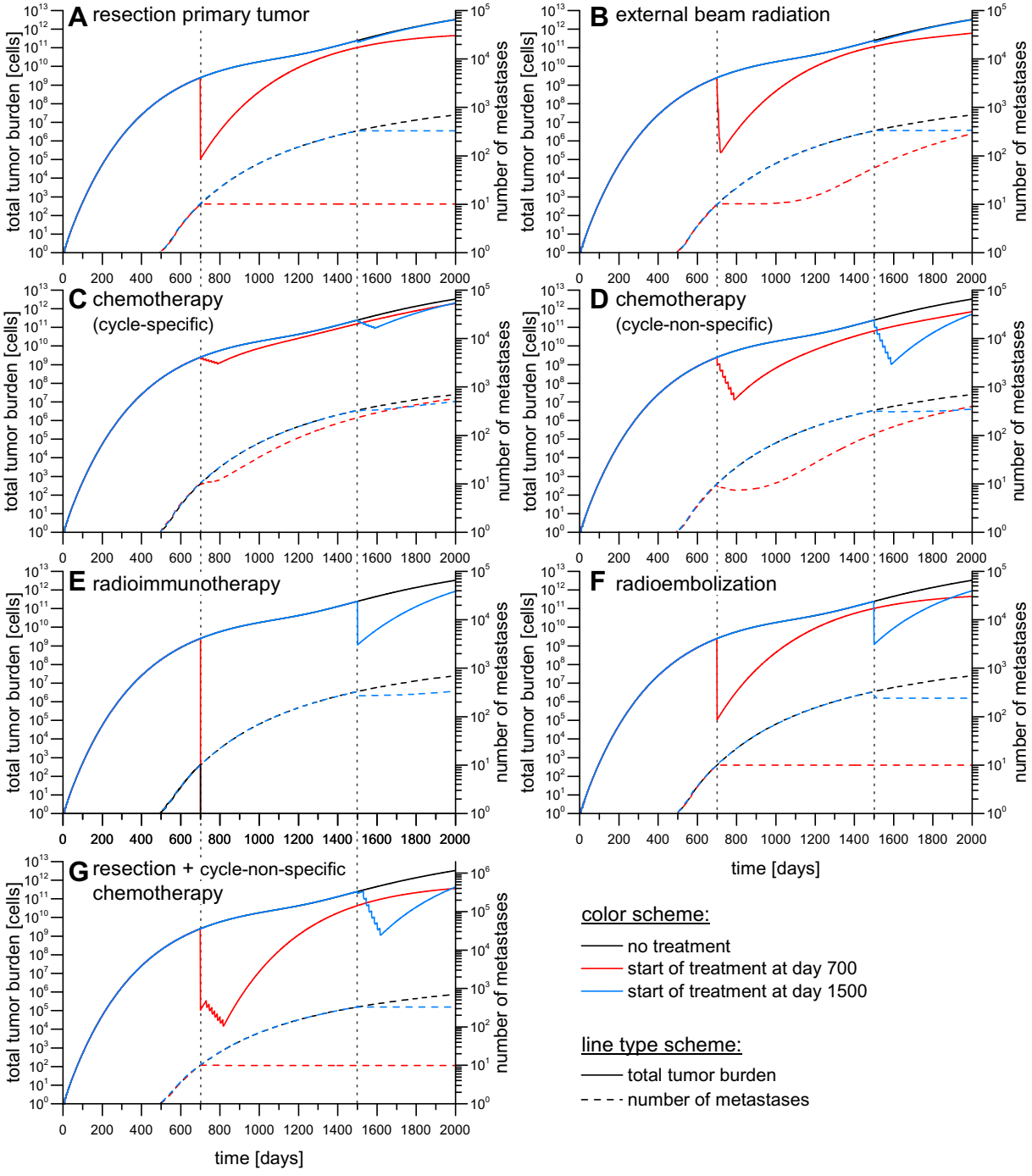

Fig. 5. Simulation results for different treatments for the simulation setups where only the primary tumor is able to spread metastases. The graphs A–G display the number of metastases (dashed lines, right *y*-axis) and the total tumor burden (solid lines, left *y*-axis) over time, for the untreated course (black lines in panels A–G) and seven simulated treatments: (A) resection of the primary tumor (PT), (B) EBRT of the primary tumor, (C) cycle-specific chemotherapy, (D) cycle-nonspecific chemotherapy, (E) radioimmunotherapy, (F) radioembolization, and (G) a combination of primary tumor resection and cycle-nonspecific chemotherapy. Treatments were started shortly after diagnosis of the primary tumor on day 700 (red lines) and once on day 1500 (blue lines). In the panels A and B the untreated course is masked by the simulation results of the treatment started at day 1500. (For interpretation of the references to color in this figure legend, the reader is referred to the web version of this article.)

However, like cycle-specific chemotherapy, it primarily affects the number of metastases indirectly, by reducing the number of cells in the primary tumor and the surviving metastases and thus slowing down the creation of new metastases (Figs. 4C–D and 5C–D).

Radioembolization can completely eradicate the primary tumor, but if treatment occurs early, the existing metastases are still too small to be detected and are therefore not affected by the treatment. Hence, in the early treatment case, radioembolization yields results similar to those for resection of the primary tumor (Figs. 4F and 5F). On day 1500, about 102 metastases ($\sigma = 7$) (metastases do metastasize) or 95 metastases ($\sigma = 6$) (metastases do not metastasize) have a diameter of 5 mm or greater and are potentially detectable clinically. They are therefore included in the treatment and are also completely eliminated like

the primary tumor. Thus, the total tumor burden can be decreased considerably in contrast to resection of the primary tumor or EBRT of the primary tumor (Figs. 4F and 5F).

If radioimmunotherapy is applied early while the primary tumor and metastases are still relatively small, it has the potential to completely eliminate the primary tumor and all metastases (Figs. 4E and 5E). If applied later in the progression of the disease, radioimmunotherapy can still reduce the number of cells considerably, although not as effectively as radioembolization (Figs. 4E–F and 5E–F), and it cannot eliminate the primary tumor. Because radioimmunotherapy also affects small metastases, this treatment can eliminate more metastases than radioembolization. However, because the primary tumor is not eradicated, the number of metastases soon starts rising again. Radioimmunotherapy has also been simulated with a varying clearance fraction of 0 (the whole administered activity is delivered to the tumor cells) and 0.95 (only 5% of the administered activity is delivered to the tumor cells). The results for early applied therapy do not differ from the results with an applied clearance fraction of 0.9 as shown in Figs. 4 and 5: the primary tumor and all metastases were completely eliminated. If radioimmunotherapy was applied late, different clearance fractions lead to different results in the number of metastases and total tumor burden (see Fig. S2 in the Supplementary Material). The results show that even in late applied therapy the same amount of activity still has the potential to eliminate the primary tumor and all metastases if the complete administered activity could be delivered to the site of the tumors.

Combination therapy involving primary tumor resection and cycle-nonspecific chemotherapy shows the most promising results if applied early (Figs. 4G and 5G). The combination therapy can reduce the tumor burden to some 10,000 cells, but as with the other types of therapy, the tumor burden starts rising again if no further treatments are applied. Again, these simulation results show the ideal case for the primary tumor resection. Simulation results for a remnant fraction of 0.1% are shown in Fig. S3 in the Supplemental Materials.

These results illustrate, in a quantitative manner, the importance of early diagnosis and the continuation of a treatment strategy even if no metastases are detectable after the first treatment cycle.

4. Discussion

CaTSiT is constructed using compartments and events as building blocks to describe the behavior of a tumor progression and metastasis system. This approach makes this tool very flexible and allows researchers to create, simulate and analyze a wide variety of setups including those ones relevant to cancer therapy. Different growth and spreading behaviors can be assigned to the primary tumor and metastases – and even to different types of metastases (e.g. lung, liver or bone metastases). Thus, different models of tumor progression and metastatic behavior (such as early or late metastasis, linear or parallel progression) can be examined with one computer model, which facilitates the comparison of those different models.

In contrast to hitherto published models, such as for example Iwata [5] or Benzekry [12], CaTSiT thereby uses a discrete event simulation approach, which inter alia allows simulating variance. Hence, instead of providing just one single result, multiple simulation runs of the same simulation setup result in a range of varying outcomes as it would also appear in real biological systems.

Furthermore, CaTSiT can also simulate tumor growth and metastatic progression under the influence of three main types of cancer therapy – primary tumor resection, chemotherapy and radiation therapy – and all these treatments can be combined in a single simulation setup. To our knowledge, no existing mathematical or computational model can accommodate this extensive and realistic kind of analysis. Existing models address either radiation therapy [26,29,30,41] or chemotherapy [17,20–22,24,60–62] (alone or in combination with primary tumor resection, immunotherapy or antiangiogenic drugs), but not both.

Since the characteristics of the different compartments, events and treatment regimens are defined in a specially developed XML file, CaTSiT can be used without the necessity of profound programming or mathematical skills, which makes it suitable for a wide range of applications in an easy way. This easy access is supported by the XSD which can be used to validate the configuration files while editing.

The building-block structure also enables straightforward extension and enhancement of the computer model. New findings and further therapies can easily be incorporated into the software. For instance, the implementation of remnants left in the tissue during the resection of the primary tumor took less than four hours. Of course, the time to implement new characteristics or treatments depends strongly on their complexity but this example nicely demonstrates how promptly the model and the CaTSiT software can be extended.

4.1. Modeling tumor dormancy

In his model, Benzekry [12] used a dynamic maximal tumor size (see Eq. (2)): the carrying capacity. He modeled dormancy by introducing extra parameters to describe the production, efficacy and elimination of angiogenesis inhibitors that influence the carrying capacity of the tumor and therefore allow or limit its growth. CaTSiT includes dormancy by replacing the current growth function with a constant function. This simplified approach has the advantage that no new mathematical terms and parameters have to be introduced, apart from parameterization of the starting size and duration of the dormancy phase.

4.2. Parametrization

Obviously, the results of the simulation depend strongly on the parametrization of the growth and spreading behavior of the primary tumor and the metastases and the parametrization of the treatments. While the dosage and frequency of drugs or radiation therapy is mostly predefined by treatment regimens and therefore won't vary strongly between patients in similar stages of the disease, the initial parameter of tumor growth and spreading behavior can vary greatly from one patient to another. Variation in only one parameter may lead to very different courses in the development of metastases and the total tumor burden. For example, as already demonstrated in [32], applying a higher growth rate to the metastases as to the primary tumor (+50% and +100%) for this one patient resulted in a significantly higher number of metastases, in the simulation setups where metastases were able to metastasize.

Concerning therapies, not only dosage and frequency but also tissue related parameter such as the proportion of cells in cycle, radiosensitivity of tumor cells or the ability to deliver drugs to the tumor cells influence the efficiency of the treatment. Exemplarily, for radioimmunotherapy, variation was simulated for the clearance fraction (0, 0.9 and 0.95) and the radio sensitivity parameters α and β (±20%). In both examples the simulation results do not differ for the case that treatment is started early at day 700: the primary tumor and all metastases are still completely eliminated. At day 1500 the clearance fraction has a great impact on the results (see Fig. S2). As already stated in the results section the same amount of administered activity lead to the complete elimination of the primary tumor and all metastases if the value

of the clearance fraction was changed from 0.9 to 0. Changing the value from 0.9 to 0.95 resulted in a clearly recognizable higher number of metastases and total tumor burden (see Fig. S2). Increasing or decreasing the radiosensitivity parameters α and β by 20% also resulted in a recognizable lower or higher number of metastases and total tumor burden (see Fig. S4) as the radiosensitivity parameters influenced the number of cells which got killed during radiation therapy. However, in comparison, α and β have less impact on the simulation results than the clearance fraction.

4.3. Limitations of the computer model

As shown in [32] and [34], CaTSiT can simulate an untreated course of tumor progression and metastasis that is in good quantitative agreement with both clinical [32] and experimental [34] data. However, because it uses a coarse-grained approach, it does not incorporate every detail. For instance, it does not differentiate between resistant and nonresistant cells, as Birkhead [16,17] did in his model for chemotherapy. Birkhead introduced five parameters to describe the rates at which cells switch between cycling and resting phases, divide, are killed, and gain resistance to cytotoxic drugs. In contrast, CaTSiT uses only three parameters to describe the effects of cytotoxic drugs; this facilitates the parameterization, but as a consequence the simulated treatments represent ideal courses and do not include any resistances that may arise during chemotherapy.

CaTSiT does not consider the influence of radiation therapy on normal tissue. Hence, treatment strategies that seem promising in the simulation results may not be feasible in vivo owing to potential increased damage to normal tissue.

At present, EBRT in our model is only available for the primary tumor. In the computer model the tumor and metastases are not given a specific location, except for "somewhere in this organ", so currently it is not possible to simulate the application of treatment to only a few metastases in a specified area of an organ.

During simulation of radioembolization treatment, the same activity is applied to each treated tumor regardless of its size; it is currently not possible to parameterize different activities for different tumors. Hence, depending on the number of treated metastases, the applied activity may exceed the maximum level tolerated in the affected organ.

The different treatments can be combined at will in CaTSiT, with one exception: radiation therapy cannot be applied directly after chemotherapy. During chemotherapy a completely different growth function is used that describes the influence of the chemotherapeutic drug on each tumor over time. Applying radiation therapy immediately after chemotherapy would require setting up a new model that can describe the effects of both therapies combined. Hence, for the time being, in the simulation radiation therapy can only be applied after the chemotherapy drug has worn off, resetting the growth function to its initial form in the process.

The implementation of the chemotherapy and radiation therapy has not yet been validated with clinical or experimental data and will need further examination by applying it to experimental data from xenograft models and clinical data from many more patients. Since this is beyond the focus of this manuscript, this approach will be modeled in subsequent work. Until now, usage of CaTSiT has been limited to analyzing data from one untreated patient [32] and from a xenograft experiment where no treatments were applied [34]. Nevertheless, in these settings the computer model has been able to provide some important insights.

CaTSiT has considerable strengths. Since it is possible to run many different simulation setups under the same computer model, CaTSiT can be used in a broad range of fields, enabling us to analyze data in a more sophisticated way. Characteristics and patterns can be discovered that classical statistical analyses cannot reveal, as shown for instance in [34]. CaTSiT can also be used to compare different models of cancer growth, as shown in [32], to estimate the number of metastases not yet detectable, and to predict the impact of various treatments on the primary tumor and metastases, in order to plan optimal treatment schedules. Furthermore, it can easily be extended to include further characteristics and new treatments.

In current research we thoroughly validate the computer model by applying it to the experimental data of different cancer cell lines, where the mice were treated either with chemotherapy, radiation therapy or a combination of chemo and radiation therapy.

Furthermore, since it is quite common in chemotherapy and radiation therapy for a certain amount of tumor cells to be resistant and/or develop resistances during the course of treatment, it is planned in the near future to extend the computer model to model these resistances as well.

5. Conclusion

CaTSiT provides an important and easy-to-use tool for analyzing data and investigating the progress of tumor growth and metastasis formation in combination with different treatment options. Future plans include application of CaTSiT to a larger collection of clinical and experimental data. By publishing CaTSiT, we want to give access of our modeling tool to the research community to use it to do similar modeling for research and to further enhance its modeling capacities.

Conflict of interest

The authors declare that they have no conflicts of interest.

Acknowledgments

AB would like to thank Prof. Dr. Andreas Wree for supervision and support and Dr. Dr. Thorsten Frenzel for helpful discussions about radiation therapy. We thank Michael Suhr for implementation of the XML configuration and Anna Sharman and Cofactor Ltd for critical reading of the manuscript.

The work of AB was supported by the European Social Fund through a scholarship from the State Graduate Funding Program (Landesgraduiertenförderung) of the University of Rostock. The funders had no involvement in study design, the collection, analysis and interpretation of data, the decision to publish, or preparation of the manuscript.

Appendix A. Supplementary material

Supplementary data associated with this article can be found, in the online version, at http://dx.doi.org/10.1016/j.jbi.2015.07.011.

References

[1] D. Hanahan, R.A. Weinberg, The hallmarks of cancer, Cell 100 (2000) 57–70.
[2] D. Hanahan, R.A. Weinberg, Hallmarks of cancer: the next generation, Cell 144 (2011) 646–674, http://dx.doi.org/10.1016/j.cell.2011.02.013.
[3] S. Valastyan, R.A. Weinberg, Tumor metastasis: molecular insights and evolving paradigms, Cell 147 (2011) 275–292, http://dx.doi.org/10.1016/j.cell.2011.09.024.
[4] C.L. Chaffer, R.A. Weinberg, A perspective on cancer cell metastasis, Science 331 (2011) 1559–1564, http://dx.doi.org/10.1126/science.1203543.
[5] K. Iwata, K. Kawasaki, N. Shigesada, A dynamical model for the growth and size distribution of multiple metastatic tumors, J. Theor. Biol. 203 (2000) 177–186, http://dx.doi.org/10.1006/jtbi.2000.1075.
[6] J. Struckmeier, A mathematical investigation of a dynamical model for the growth and size distribution of multiple metastatic tumors, Universität Hamburg, Hamburger Beiträge Zur Angewandten Mathematik, 2003.

[7] D. Barbolosi, A. Benabdallah, F. Hubert, F. Verga, Mathematical and numerical analysis for a model of growing metastatic tumors, Math. Biosci. 218 (2009) 1–14, http://dx.doi.org/10.1016/j.mbs.2008.11.008.
[8] A. Devys, T. Goudon, P. Lafitte, A model describing the growth and the size distribution of multiple metastatic tumors, DCDS-B 12 (2009) 731–767, http://dx.doi.org/10.3934/dcdsb.2009.12.731.
[9] V. Haustein, U. Schumacher, A dynamic model for tumour growth and metastasis formation, J. Clin. Bioinform. 2 (2012) 11, http://dx.doi.org/10.1186/2043-9113-2-11.
[10] N. Hartung, S. Mollard, D. Barbolosi, A. Benabdallah, G. Chapuisat, G. Henry, et al., Mathematical modeling of tumor growth and metastatic spreading: validation in tumor-bearing mice, Cancer Res. (2014), http://dx.doi.org/10.1158/0008-5472.CAN-14-0721. canres.0721.2014.
[11] S. Benzekry, Mathematical analysis of a two-dimensional population model of metastatic growth including angiogenesis, J. Evol. Equ. 11 (2011) 187–213, http://dx.doi.org/10.1007/s00028-010-0088-5.
[12] S. Benzekry, A. Gandolfi, P. Hahnfeldt, Global dormancy of metastases due to systemic inhibition of angiogenesis, PLoS ONE 9 (2014) e84249, http://dx.doi.org/10.1371/journal.pone.0084249.
[13] P.K. Newton, J. Mason, K. Bethel, L.A. Bazhenova, J. Nieva, P. Kuhn, A stochastic Markov chain model to describe lung cancer growth and metastasis, PLoS ONE 7 (2012) e34637, http://dx.doi.org/10.1371/journal.pone.0034637.
[14] P.K. Newton, J. Mason, K. Bethel, L. Bazhenova, J. Nieva, L. Norton, et al., Spreaders and sponges define metastasis in lung cancer: a Markov chain mathematical model, Cancer Res. 73 (2013) 2760–2769, http://dx.doi.org/10.1158/0008-5472.CAN-12-4488.
[15] T.E. Wheldon, Models of tumour response to chemotherapy, in: Mathematical Models in Cancer Research, Adam Hilger, Bristol, 1988, pp. 157–179.
[16] B.G. Birkhead, W.M. Gregory, A mathematical model of the effects of drug resistance in cancer chemotherapy, Math. Biosci. 72 (1984) 59–69, http://dx.doi.org/10.1016/0025-5564(84)90061-0.
[17] B.G. Birkhead, E.M. Rankin, S. Gallivan, L. Dones, R.D. Rubens, A mathematical model of the development of drug resistance to cancer chemotherapy, Eur. J. Cancer Clin. Oncol. 23 (1987) 1421–1427, http://dx.doi.org/10.1016/0277-5379(87)90133-7.
[18] J.R. Usher, Some mathematical models for cancer chemotherapy, Comput. Math. Appl. 28 (1994) 73–80, http://dx.doi.org/10.1016/0898-1221(94)00179-0.
[19] J.C. Panetta, A logistic model of periodic chemotherapy, Appl. Math. Lett. 8 (1995) 83–86, http://dx.doi.org/10.1016/0893-9659(95)00053-S.
[20] J.C. Panetta, A mathematical model of periodically pulsed chemotherapy: tumor recurrence and metastasis in a competitive environment, Bull. Math. Biol. 58 (1996) 425–447, http://dx.doi.org/10.1007/BF02460591.
[21] J.C. Panetta, J. Adam, A mathematical model of cycle-specific chemotherapy, Math. Comput. Model. 22 (1995) 67–82, http://dx.doi.org/10.1016/0895-7177(95)00112-F.
[22] P. Dua, V. Dua, E.N. Pistikopoulos, Optimal delivery of chemotherapeutic agents in cancer, Comput. Chem. Eng. 32 (2008) 99–107, http://dx.doi.org/10.1016/j.compchemeng.2007.07.001.
[23] A. D' Onofrio, U. Ledzewicz, H. Maurer, H. Schättler, On optimal delivery of combination therapy for tumors, Math. Biosci. 222 (2009) 13–26, http://dx.doi.org/10.1016/j.mbs.2009.08.004.
[24] S. Benzekry, G. Chapuisat, J. Ciccolini, A. Erlinger, F. Hubert, A new mathematical model for optimizing the combination between antiangiogenic and cytotoxic drugs in oncology, C.R. Math. 350 (2012) 23–28, http://dx.doi.org/10.1016/j.crma.2011.11.019.
[25] L.G. De Pillis, W. Gu, A.E. Radunskaya, Mixed immunotherapy and chemotherapy of tumors: modeling, applications and biological interpretations, J. Theor. Biol. 238 (2006) 841–862, http://dx.doi.org/10.1016/j.jtbi.2005.06.037.
[26] P. Wang, Y. Feng, A mathematical model of tumor volume changes during radiotherapy, Sci. World J. 2013 (2013) 181070, http://dx.doi.org/10.1155/2013/181070.
[27] P. Bernhardt, H. Ahlman, E. Forssell-Aronsson, Model of metastatic growth valuable for radionuclide therapy, Med. Phys. 30 (2003) 3227, http://dx.doi.org/10.1118/1.1628851.
[28] P. Bernhardt, H. Ahlman, E. Forssell-Aronsson, Modelling of metastatic cure after radionuclide therapy: influence of tumor distribution, cross-irradiation, and variable activity concentration, Med. Phys. 31 (2004) 2628, http://dx.doi.org/10.1118/1.1786531.
[29] T.E. Wheldon, Radiotherapy: treatment strategies, in: Mathematical Models in Cancer Research, Adam Hilger, Bristol, 1988, pp. 134–156.
[30] K. Leder, K. Pitter, Q. LaPlant, D. Hambardzumyan, B.D. Ross, T.A. Chan, et al., Mathematical modeling of PDGF-driven glioblastoma reveals optimized radiation dosing schedules, Cell 156 (2014) 603–616, http://dx.doi.org/10.1016/j.cell.2013.12.029.
[31] K. Leder, J. Ramakrishnan, Minimizing metastatic risk in radiotherapy fractionation schedules. Available from: arXiv:13127337 [physics, Q-Bio] 2013.
[32] A. Bethge, U. Schumacher, A. Wree, G. Wedemann, Are metastases from metastases clinical relevant? Computer modelling of cancer spread in a case of hepatocellular carcinoma, PLoS ONE 7 (2012) e35689, http://dx.doi.org/10.1371/journal.pone.0035689.
[33] C.A. Klein, Parallel progression of primary tumours and metastases, Nat. Rev. Cancer 9 (2009) 302–312, http://dx.doi.org/10.1038/nrc2627.
[34] T. Brodbeck, N. Nehmann, A. Bethge, G. Wedemann, U. Schumacher, Perforin-dependent direct cytotoxicity in natural killer cells induces considerable knockdown of spontaneous lung metastases and computer modelling-proven tumor cell dormancy in a HT29 human colon cancer xenograft mouse model, Mol. Cancer (2014).
[35] G. Wedemann, A. Bethge, V. Haustein, U. Schumacher, Computer simulation of the metastatic progression, in: Metastasis Research Protocols, second ed., Springer, New York, 2014, pp. 107–116.
[36] R.A. Weinberg, The Nature of Cancer. The Biology of Cancer, Garland Science, 2006. pp. 25–56.
[37] R.A. Weinberg, Moving Out: Invasion and Metastasis. The Biology of Cancer, Garland Science, 2006. pp. 587–654.
[38] J.E. Talmadge, B. Zbar, Clonality of pulmonary metastases from the bladder 6 subline of the B16 melanoma studied by southern hybridization, J. Natl Cancer Inst. 78 (1987) 315–320.
[39] M. Matsumoto, T. Nishimura, Mersenne twister: a 623-dimensionally equidistributed uniform pseudo-random number generator, ACM Trans. Model. Comput. Simul. 8 (1998) 3–30, http://dx.doi.org/10.1145/272991.272995.
[40] A. Caley, R. Jones, The principles of cancer treatment by chemotherapy, Surgery (Oxford) 30 (2012) 186–190, http://dx.doi.org/10.1016/j.mpsur.2012.01.004.
[41] P. Bernhardt, T.W. Speer, Modeling of the systemic cure with targeted radionuclide therapy, in: T.W. Speer (Ed.), Targeted Radionuclide Therapy, Lippincott Williams and Wilkins, 2010, pp. 263–281.
[42] R.M. Sharkey, D.M. Goldenberg, Perspectives on cancer therapy with radiolabeled monoclonal antibodies, J. Nucl. Med. 46 (2005) 115S–127S.
[43] D.E. Milenic, E.D. Brady, M.W. Brechbiel, Antibody-targeted radiation cancer therapy, Nat. Rev. Drug Discov. 3 (2004) 488–499, http://dx.doi.org/10.1038/nrd1413.
[44] M. Heine, P. Nollau, C. Masslo, P. Nielsen, B. Freund, O.T. Bruns, et al., Investigations on the usefulness of CEACAMs as potential imaging targets for molecular imaging purposes, PLoS ONE 6 (2011) e28030, http://dx.doi.org/10.1371/journal.pone.0028030.
[45] M. Heine, B. Freund, P. Nielsen, C. Jung, R. Reimer, H. Hohenberg, et al., High interstitial fluid pressure is associated with low tumour penetration of diagnostic monoclonal antibodies applied for molecular imaging purposes, PLoS ONE 7 (2012) e36258, http://dx.doi.org/10.1371/journal.pone.0036258.
[46] R. Loevinger, T.F. Budinger, E.E. Watson, MIRD Primer for Absorbed Dose Calculations, revised ed., Society of Nuclear Medicine, 1991.
[47] W.S. Snyder, M.R. Ford, G.G. Warner, S.B. Watson, MIRD Pamphlet No. 11: "S" Absorbed Dose per Unit Cumulated Activity for Selected Radionuclides and Organs, Society of Nuclear Medicine, 1975.
[48] A. Kennedy, J. Welsh, Radioembolization with Yttrium-90 microspheres for primary and metastatic hepatic cancer, in: T.W. Speer (Ed.), Targeted Radionuclide Therapy, Lippincott Williams and Wilkins, 2010, pp. 305–317.
[49] R. Salem, R.J. Lewandowski, M.F. Mulcahy, A. Riaz, R.K. Ryu, S. Ibrahim, et al., Radioembolization for hepatocellular carcinoma using Yttrium-90 microspheres: a comprehensive report of long-term outcomes, Gastroenterology 138 (2010) 52–64, http://dx.doi.org/10.1053/j.gastro.2009.09.006.
[50] A. Akanuma, Parameter analysis of Gompertzian function growth model in clinical tumors, Eur. J. Cancer 14 (1978) 681–688.
[51] M.H. Pourgholami, L. Woon, R. Almajd, J. Akhter, P. Bowery, D.L. Morris, In vitro and in vivo suppression of growth of hepatocellular carcinoma cells by albendazole, Cancer Lett. 165 (2001) 43–49, http://dx.doi.org/10.1016/S0304-3835(01)00382-2.
[52] Patrick G. Morris, Teresa A. Gilewski, Larry Norton, Norton-Simon hypothesis, in: Michael C. Perry (Ed.), Perry's The Chemotherapy Source Book, fifth ed., LWW, Philadelphia, 2012, pp. 8–27.
[53] K.K. Chan, J.L. Cohen, J.F. Gross, K.J. Himmelstein, J.R. Bateman, Y. Tsu-Lee, et al., Prediction of adriamycin disposition in cancer patients using a physiologic, pharmacokinetic model, Cancer Treat. Rep. 62 (1978) 1161–1171.
[54] A. Tai, B. Erickson, K.A. Khater, X.A. Li, Estimate of radiobiologic parameters from clinical data for biologically based treatment planning for liver irradiation, Int. J. Radiat. Oncol. Biol. Phys. 70 (2008) 900–907, http://dx.doi.org/10.1016/j.ijrobp.2007.10.037.
[55] Z.-C. Zeng, Z.-Y. Tang, B.-H. Yang, K.-D. Liu, Z.-Q. Wu, J. Fan, et al., Comparison between radioimmunotherapy and external beam radiation therapy for patients with hepatocellular carcinoma, Eur. J. Nucl. Med. Mol. Imag. 29 (2002) 1657–1668, http://dx.doi.org/10.1007/s00259-002-0996-x.
[56] C.J. Huang, S.L. Lian, S.C. Chen, D.K. Wu, S.Y. Wei, M.Y. Huang, et al., External beam radiation therapy for inoperable hepatocellular carcinoma with portal vein thrombosis, Kaohsiung J. Med. Sci. 17 (2001) 610–614.
[57] A.C. Cupino, C.D. Hair, J.F. Angle, S.H. Caldwell, T.A. Rich, C.L. Berg, et al., Does external beam radiation therapy improve survival following transarterial chemoembolization for unresectable hepatocellular carcinoma?, Gastrointest Cancer Res 5 (2012) 13–17.
[58] K.F. Eckerman, K.F.E. Endo, A. Endo, MIRD: Radionuclide Data and Decay Schemes, SNMMI, 1989.
[59] G.H. Kramer, B.M. Hauck, M.J. Chamberlain, Biological half-life of Iodine in adults with intact thyroid function and in athyreotic persons, Radiat. Prot. Dosimetry. 102 (2002) 129–135.
[60] S. Benzekry, N. André, A. Benabdallah, J. Ciccolini, C. Faivre, F. Hubert, et al., Modeling the impact of anticancer agents on metastatic spreading, Math.

Model. Nat. Phenom. 7 (2012) 306–336, http://dx.doi.org/10.1051/mmnp/20127114.

[61] S. Benzekry, P. Hahnfeldt, Maximum tolerated dose versus metronomic scheduling in the treatment of metastatic cancers, J. Theor. Biol. 335 (2013) 235–244, http://dx.doi.org/10.1016/j.jtbi.2013.06.036.

[62] D. Barbolosi, A. Benabdallah, S. Benzekry, J. Ciccolini, C. Faivre, F. Hubert, et al., A mathematical model for growing metastases on oncologists's service, in: M. Garbey, B.L. Bass, S. Berceli, C. Collet, P. Cerveri (Eds.), Computational Surgery and Dual Training, Springer, New York, 2014, pp. 331–338.